The Movement of Spermatozoa with Helical Head: Theoretical Analysis and Experimental Results

F. Andrietti and G. Bernardini
Dipartimento di Biologia, Università di Milano, Milano, Italy

ABSTRACT The present work is concerned with the study of the swimming of flagellated microscopic organisms with a helical head and a helical pattern of flagellar beating, such as *Xenopus* sperms. The theoretical approach is similar to that taken by Chang and Wu (1971) in the study of helical flagellar movement. The model used in the present study allows us to determine the velocity of propulsion (U) and the frequency of rotation of the sperm head (f_h) as a function of the frequency of the wave of motion (f_t) traveling along the tail. The results relative to the case of helical and planar flagellar waves are compared. Our main finding is that the helical shape of the head seems to increase the efficiency of propulsion of the spermatozoon when compared with the more commonly shaped spherical head. Experimentally measured values of f_h versus U may be fitted by a linear plot whose slope is much higher than that corresponding to the case of a planar flagellar beating. This fact is consistent with an effectively three-dimensional (nonplanar) movement of the flagellar tail. However, the results do not fit those predicted from a circular helix, suggesting that a different shape of the flagellar beating should be considered.

INTRODUCTION

Helical shape is a feature largely scattered among unrelated microscopic organisms; fern spermatozoids, spirilla, some Phytoflagellata, and *Xenopus* sperms are a few examples. The analysis of their movement has been performed by means of hydrodynamic (Lowndes, 1943; Brown, 1945; Chwang et al., 1972) and mathematical models (Hollwill, 1966; Mysercough and Swan, 1989). One of the points stressed by such studies concerns the contribution of the body shape to the movement of the organisms. However, the works mentioned were concerned either with the case of spirilla (Chwang et al., 1972; Mysercough and Swan, 1989) or *Euglena* (Holwill, 1966). A spirillar locomotory apparatus consists of one or more bundles of flagella at the end of the body, beating on a conical surface of revolution. *Euglena* is not comparable with *Xenopus* sperms either in locomotory apparatus or in body shape. Because both cases are different from that presented by *Xenopus* sperms, this requires a quite different analysis. In fact these organisms are very thin cells with a corkscrew shape of the head and a helical, three-dimensional flagellar beating. They move following a path which is, at least approximately, straight.

The aim of the present work is to investigate the movement of *Xenopus* spermatozoa by making use of a simple theory and to relate the results of the theoretical study with the experimental data obtained by the video recording of the swimming of the sperms reported in a previous paper (Bernardini et al., 1988), in which a description of the experimental method used in this study appears.

Received for publication 21 April 1994 and in final form 26 July 1994.

Address reprint requests to Dr. F. Andrietti, Dipartimento di Biologia, Università Degli Studi di Milano, Via Celoria 26, 20133 Milano, Italy. Tel.: 39 226604460; Fax: 39 22361070.

0006-3495/94/10/1767/08 $2.00

THEORY

Helical flagellar wave

We will consider the case of a sperm moving uniformly with a translational movement U and rotating around its axis with an angular velocity Ω_h. Dealing with helical structures, it is suitable to use cylindrical coordinates. We will consider a system of such coordinates, (r, θ, x), fixed to the sperm head, with the origin in the point of attachment of the tail and the x-axis coincident with that of the head and the tail, pointing toward the end of the tail (Fig. 1).

In these coordinates the head is described as

$$r = h_h \qquad \theta = -k_h \chi, \tag{1}$$

where h_h is the head radius, $k_h = 2\pi/\delta_h$ is the head wave number and δ_h its wave length.

In the same coordinate system the flagellar tail movement is described as

$$r = h_t$$
$$\theta = k_t x + (\Omega_t - \Omega_h)t = k_t x + (k_t c_t - \Omega_h)t \tag{1'}$$

where h_t is the radial amplitude of the helical wave of the tail, δ_t its wave length, $k_t = 2\pi/\delta_t$ the tail wave number, Ω_t the velocity of rotation of the flagellar tail with respect to a fixed frame of reference, $\Omega_t - \Omega_h$ the apparent tail angular velocity, and $c_t = \Omega_t/k_t$ the phase velocity of the wave of motion traveling along the tail.

By applying the Gray and Hancock theory (1955) to the case of helical structures we have for the tail (Chwang and Wu, 1971)

$$dF_{t,n} = C_{t,n}[(k_t c_t - \Omega_h)h_t - Uk_t h_t]\,dx \tag{3}$$

and

$$dF_{t,s} = C_{t,s}[(k_t c_t - \Omega_h)k_t h_t^1 + U]\,dx \tag{4}$$

where $F_{t,n}$, $F_{t,s}$, $C_{t,n}$, $C_{t,s}$ are the tail normal (n) and tangential (s) forces and coefficients of resistance, respectively.

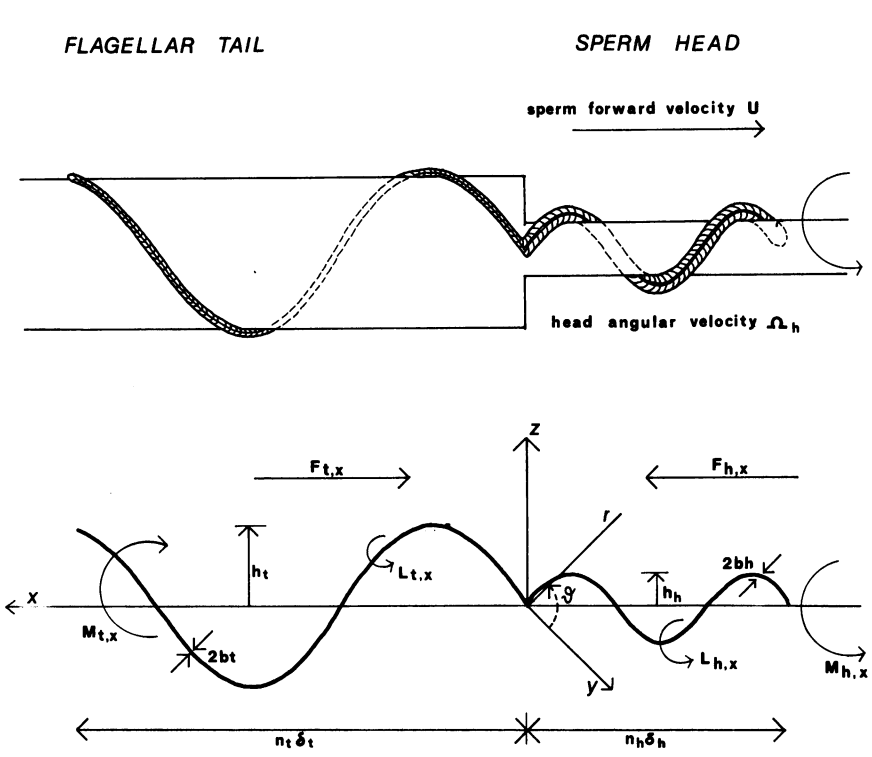

FIGURE 1 Schematic diagram of a spermatozoon with a helical head and a helical flagellar tail. For explanation of symbols and values of parameters see Table 1.

By analogy, we obtain for the head

$$dF_{h,n} = C_{h,n}[-\Omega_h h_h - Uk_h h_h]dx \tag{3'}$$

and

$$dF_{h,s} = C_{h,s}[-\Omega_h k_h h_h^2 + U]dx \tag{4'}$$

with an obvious meaning of symbols.

The propulsive force $dF_{t,x}$ originated by an element ds of the tail in the direction of the x-axis is given by Chwang and Wu (1971) as

$$dF_x = (dF_{t,n}\sin\beta_t - dF_{t,s}\cos\beta_t) \tag{5}$$

where β_t is the angle between the tail and the x-axis given by

$$\tan\beta_t = (2\pi/\delta_t)h_t = k_t h_t, \tag{6}$$

whereas the force in the Θ direction is given by

$$dF_\vartheta = -(dF_{t,n}\cos\beta_t + dF_{t,s}\sin\beta_t)$$

which, in turn, gives a moment of force about the x-axis

$$dM_{t,x} = h_t dF_{t,\vartheta} = -h_t(dF_{t,n}\cos\beta_t + dF_{t,s}\sin\beta_t) \tag{7}$$

The total propulsive force and torque is given by integration of Eqs. 5 and 7 between $x = 0$ and $x = n_t\delta_t$, where n_t is the number of flagellar wavelengths.

According to Gray and Hancock (1955), the force coefficients are given by

$$C_{i,n} = 2C_{i,s} \qquad i = t, h \tag{8}$$

$$C_{i,s} = 2\pi\mu/[\ln(2\delta_i/b_i) - 0.5] \qquad i = t, h \tag{9}$$

Taking into account the relationships

$$\cos\beta_t = (1 + K_t^2)^{-1/2}, \qquad \sin\beta_t = K_t(1 + K_t^2)^{-1/2}$$

where $K_t = h_t k_t$, we find by Eqs. 3, 4, 5, 7, 8,

$$F_{t,x} = \int_0^{n_t\delta_t} dF_{t,x}\,dx \tag{10}$$
$$= C_{t,s}n_t\delta_t[(k_t c_t - \Omega_h)h_t K_t^2 - U(2K_t^2 + 1)](1 + K_t^2)^{-1/2}$$

$$M_{t,x} = \int_0^{n_t\delta_t} dM_{t,x}\,dx$$
$$= C_{t,s}n_t\delta_t h_t[UK_t + \Omega_h h_t(2 + K_t^2) - K_t(2 + K_t^2)c_t]$$
$$\times (1 + K_t^2)^{-1/2} \tag{11}$$

By similar reasoning we find

$$F_{h,x} = \int_0^{n_h\delta_h} dF_{h,x}\,dx \tag{10'}$$
$$= C_{h,s}n_h\delta_h[-\Omega_h h_h K_h - U(2K_h^2 + 1)](1 + K_h^2)^{-1/2}$$

$$M_{h,x} = \int_0^{n_h\delta_h} dM_{h,x}\,dx \tag{11'}$$
$$= C_{h,s}n_h\delta_h h_h[UK_h + \Omega_h h_h(2 + K_h^2)](1 + K_h^2)^{-1/2}$$

with obvious meaning of symbols not yet defined. Observe that $F_{h,x}$ and $M_{h,x}$ have the meaning of head viscous drag and torque, because of the head translational and rotational movement, respectively.

Finally, we have to consider that, as long as the sperm body rotates around the x-axis with the angular velocity Ω_h, every cross-section of the helical head also rotates around the tangent of its central curve (i.e., a line passing through the center of each cross-section), giving rise to an additional viscous torque L_h. The same is true for the tail, which gives rise to an additional viscous torque L_t (see Chwang and Wu (1971) and their Fig. 2). These additional torques are small compared with $M_{h,x}$ and $M_{t,x}$, and they are given here only for sake of completeness. The x-component $dL_{t,x}$ of the infinitesimal torque of a cylindrical tail element of radius b_t is given by Chwang and Wu (1971) and Lamb (1932).

$$dL_{t,x} = 4\pi\mu b_t^2 \Omega_h \cos\beta_t dx$$

where μ is the viscosity coefficient, so that

$$L_{t,x} = \int_0^{n_t\delta_t} dL_{t,x} = 4\pi\mu b_t^2 \Omega_h n_t \delta_t \cos\beta_t \qquad (12)$$

Analogously we find

$$L_{h,x} = 4\pi\mu b_h^2 \Omega_h n_h \delta_h \cos\beta_h \qquad (12')$$

The balance of total forces and moments in the x-direction requires

$$F_{t,x} + F_{h,x} = 0 \qquad (13)$$

$$M_{t,x} + M_{h,x} + L_{t,x} + L_{h,x} = 0 \qquad (14)$$

By Eqs. 13, 14, 10–12, and 10′–12′ we obtain

$$\begin{aligned} A_{1,5}U + A_{1,2}\Omega_h &= C_{t,s} n_t \delta_t K_t^2 c_t (1 + K_t^2)^{-1/2} \\ A_{2,1}U + A_{2,2}\Omega_h &= C_{t,s} n_t \delta_t h_t (1 + K_t^2)^{-1/2} K_t (2 + K_t^2) c_t \end{aligned} \qquad (15)$$

where

$$\begin{aligned} A_{1,1} &= C_{t,s} n_t \delta_t (2K_t^2 + 1)(1 + K_t^2)^{-1/2} \\ &\quad + C_{h,s} n_h \delta_h (2K_h^2 + 1)(1 + K_h^2)^{-1/2} \\ A_{1,s} &= C_{t,s} n_t \delta_t h_t K_t (1 + K_t^2)^{-1/2} + C_{h,s} n_h \delta_h h_h K_h (1 + K_h^2)^{-1/2} \\ A_{2,1} &= C_{t,s} n_t \delta_t h_t K_t (1 + K_t^2)^{-1/2} + C_{h,s} n_h \delta_h h_h K_h (1 + K_h^2)^{-1/2} \\ A_{2,2} &= C_{t,s} n_t \delta_t h_t^2 \left[2 + K_t^2 + \frac{4\pi\mu}{C_{t,s}} \left(\frac{b_t}{h_t} \right)^2 \right] (1 + K_t^2)^{-1/2} \\ &\quad + C_{h,s} n_h \delta_h h_h^2 \left[2 + K_h^2 + \frac{4\pi\mu}{C_{h,s}} \left(\frac{b_h}{h_h} \right)^2 \right] (1 + K_h^2)^{-1/2} \end{aligned}$$

Resolution of Eq. 15 allows determination of the unknown values Ω_h and U.

A different expression for the force coefficients developed by Lighthill (1975, p. 52) is the following, which improves on Eqs. 8 and 9.

$$C_{i,n} = \frac{8\pi\mu}{\ln(0.0324\delta_i^2/b_i^2) + 1} \qquad i = t, h \qquad (8')$$

$$C_{i,s} = \frac{4\pi\mu}{\ln(0.0324\delta_i^2/b_i^2) - 1} \qquad i = t, h \qquad (9')$$

The use of force coefficients given by Eqs. 8′–9′ gives rise to formulae not reported here, which are only slightly more complicated than the previous ones.

Planar flagellar wave

In the case of a planar wave the flagellar movement does not induce a torque. However, if the head has a helical shape, an indirect torque is produced given by Eq. 11′ or, more generally, leaving coefficients $C_{h,n}$, and $C_{h,s}$ free to assume independent values

$$\begin{aligned} M_{h,x} &= n_h \delta_h h_h^2 (1 + K_h^2)^{-1/2} \\ &\quad \times [(C_{h,n} - C_{h,s}) k_h U + (C_{h,n} + C_{h,s} K_h^2) \Omega_h] \end{aligned} \qquad (16)$$

Because of the rotation induced by the head, the tail will rotate around the x-axis with the angular velocity $\Omega = -\Omega_h$, producing a viscous torque $M'_{t,x}$. The rotation of the tail generates a force perpendicular to each tail element ds given by

$$dF_{t,n} = C_{t,n} V_{t,\theta} ds \qquad (17)$$

where $V_{t,\theta}$, the velocity of rotation of each element ds, is given by $y_t\Omega$, $y_t(x) = h_t \sin[k_t(x + c_t t)]$ is the form of the wave generated by the tail conforming to a sine curve, and

$$ds = [1 + (dy_t/dx)^2]^{1/2} dx \qquad (18)$$

From Eqs. 17 and 18 we have

$$\begin{aligned} M'_{t,x} &= \int_0^{n_t\delta_t} dM'_{t,x}\, dx = \int_0^{n_t\delta_t} y_t C_{t,n} V_{t,\theta} \left[1 + \left(\frac{dy_t}{dx} \right)^2 \right]^{1/2} dx \\ &= C_{t,n} h_t^2 \Omega \int_0^{n_t\delta_t} \sin^2[k_t(x + c_t t)] \\ &\quad \times (1 + h_t^2 k_t^2 \cos^2[k_t(x + c_t t)])^{1/2}\, dx \end{aligned}$$

The above integral is in general time-dependent, because n_t is a non-integer number. However, if we average the different values of the moment during a given period of time, phase differences will cancel and the resulting average value of the moment $\langle M'_{t,x} \rangle$ will be given by

$$\langle M'_{t,x} \rangle = n_t C_{t,n} h_t^2 \Omega \int_0^{\delta_t} \sin^2 k_t x [1 + h_t^2 k_t^2 \cos^2(k_t x)]^{1/2}\, dx$$

where now the integral is calculated at $t = 0$ and is independent of time.

The evaluation of the above integral cannot be given in closed form, but it may be expressed by means of elliptic integrals. However, an approximate value may be obtained taking into account that $\cos^2 k_t x = \frac{1}{2}[1 + \cos(4\pi/\delta_t)x]$. The second term in the brackets may be ignored in a first approximation, given that its contribution to the integral will be less than the first term. Substituting $\cos^2 k_t x \approx \frac{1}{2}$ in the square root of the integral, find

$$\langle M'_{t,x} \rangle \approx (n_t/2) C_{t,n} h_t^2 \Omega \delta_t [1 + K_t^2/2]^{1/2} \qquad (19)$$

A second viscous torque to be taken into account is again that generated by the rotation of each tail and head cross-sections around the tangent of its central curve, given by Eqs. 12 (when $\cos\beta_t = 0$) and 12′, respectively.

The balance of all moments requires

$$M_{h,x} + \langle M'_{t,x} \rangle + L_{t,x} + L_{h,x} = 0 \qquad (20)$$

In a planar flagellar beating the presence of an additional torque perpendicular to the plane of the flagellar movement should be considered. In the simplified model of Gray and Hancock (1955) that we are following here, this additional component is disregarded. It has been taken into account, instead, in more elaborate treatments such as that given by Higdon (1979). Because of this additional moment, the trajectory of the organism during one cycle of flagellar beating is represented by a yawing motion rather than by a straight line. However, for any symmetrical wave of flagellar beating such as that considered here, the organism has no net rotation over a whole cycle of flagellar beating, and the trajectory is symmetrical with respect to the direction of movement. Moreover, it has been shown (Higdon, 1979) that, at least in the case of organisms with a spherical head, when the ratio between the radius of the head and the length of the flagellar tail is higher than 20, the use of the force coefficients of Gray and Hancock (1955) gives results accurate to within 10%. In our case we are dealing with helical heads. However, the ratio between the flagellar length and the "equivalent" spherical head radius (see Table 1) is higher than 20. Moreover, the yawing motion should be less in the case of a more elongated helical head than in that of a spherical one. For all these reasons we will disregard the torque perpendicular to the plane of the flagellar beating, because this error is certainly not greater than and is probably even less than those inherent to any model based on the resistive-force theory.

By substituting Eqs. 16, 19, 12, and 12′ in Eq. 20, we may easily derive the following linear relationship between U and Ω

$$\frac{\Omega}{U} = \frac{(C_{h,s} - C_{h,n}) n_h \delta_h K_h h_h}{\{\ \}} \qquad (21)$$

where

$$\{\ \} = C_{t,n} h_t^2 (n_t/2)\delta_t [1 + (K_t^2/2)]^{1/2}(1 + K_h^2)^{1/2} + n_h \delta_h [4\pi\mu b_h^2 + h_h^2 (C_{h,n} + C_{h,s} K_h^2)] + 4\pi\mu b_t^2 n_t \delta_t (1 + K_h^2)^{1/2}$$

To evaluate Ω and U, the balance of the propulsive forces and resistances is also required. From Gray and Hancock (1955) we find that the total propulsive force along the x-axis is given by

$$c_t(C_{t,n} - C_{t,s}) \int_0^{n_t \delta_t} \left[\frac{A^2}{(1 + A^2)^{1/2}} \right] dx - U \int_0^{n_t \delta_t} \left[\frac{C_{t,s} + C_{t,n} A^2}{(1 + A^2)^{1/2}} \right] dx = I - UL$$

where $A = dy_t/dx = K_t \cos[k_t(x + c_t t)]$. The integrals I and L, when averaged with respect to time, may be calculated as

$$\langle I \rangle = n_t c_t (C_{t,n} - C_{t,s}) \int_0^{\delta_t} \left[\frac{K_t^2 \cos^2 k_t x}{(1 + K_t^2 \cos^2 k_t x)^{1/2}} \right] dx \qquad (22)$$

$$\langle L \rangle = n_t \int_0^{\delta_t} \left[\frac{C_{t,s} + C_{t,n} K_t^2 \cos^2 k_t x}{(1 + K_t^2 \cos^2 k_t x)^{1/2}} \right] dx \qquad (23)$$

TABLE 1 Meaning of symbols and values of experimental data

i	= index related to the flagellar tail (t) or the sperm head (h)
ω_i	= angular velocity
$F_{i,n}$; $F_{i,s}$; $F_{i,x}$; $F_{i,\theta}$	= normal, tangential, x-directed and θ directed forces
$M_{i,x}$	= torque component in the x-direction
$C_{i,n}$; $C_{i,t}$	= normal and tangential force coefficients
β_i	= angle between helical tail or head and x-direction
k_i	= wave number $= 2\pi/\delta_i$
K_i	= $h_i k_i$
$L_{i,x}$	= torque induced by the rotation of each cross section of tail or head sections around its central curve
l_t (flagellar length)	= 40 μm*
δ_t (flagellar wavelength)	= 19.2 μm
n_t (number of wavelengths along the flagellum)	= 1.22
h_t (wave amplitude of the flagellar wave central curve)	= $(l_t^2 - n_t^2\delta_t^2)^{1/2}/2\pi n_t$ = 4.3 μm, for helical waves
	= $(\delta_t/\pi\sqrt{2})[l_t/(n_t\delta_t - 1)]^{1/2}$ = 3.6 μm, for planar waves
b_t (flagellar cross-sectional radius)	= 0.1 μm
l_h (helical head length)	= 22 μm*
δ_h (helical head wavelength)	= 9.2 μm
n_h (number of wavelengths along the helica head)	= 1.5*
h_h (wave amplitude of the helical head central curve)	= $(l_h^2 - n_h^2\delta_h^2)^{1/2}/2\pi n_h$ = 1.82 μm
b_h (helical head cross-sectional radius)	= 0.4 μm*
f_h (frequency of gyration of the helical head)	= 0.5 Hz
f_t (frequency of flagellar movement)	= 1.0 Hz
f (apparent frequency of gyration of the tail)	= 0.5 Hz
a (radius of the equivalent spherical head)	= $[\frac{3}{4} b_h^2 l_h]^{1/3}$ = 1.38 μm

* Bernardini et al. (1988); all other data are from unpublished results.

The balance of forces in the x-direction requires $\langle I\rangle - U\langle L\rangle + F_{h,x} = 0$. When $F_{h,x}$ is given by Eq. 10′ generalized to the case when $C_{h,n}$ and $C_{h,s}$ are independent values, we obtain from the balance equation

$$[(C_{h,n}K_h^2 + C_{h,s})(1 + K_h^2)^{-1/2}n_h\delta_h + \langle L\rangle]U + [K_h h_h (1 + K_h^2)^{-1/2}n_h\delta_h](C_{h,n} - C_{h,s})\Omega = \langle I\rangle \quad (25)$$

where $\langle I\rangle$ and $\langle L\rangle$ are given by Eqs. 22 and 23, respectively.

Eqs. 25 and 21 allow determination of the unknown variables U and Ω. The evaluation of integrals from Eqs. 22 and 23 may be given in terms of elliptic integrals. However, an approximate value of these integrals may be obtained as seen above. If we substitute $\cos^2 k_t x \approx \frac{1}{2}$ in the denominator of the integrals from Eqs. 22 and 23, in a first approximation they reduce to

$$\langle I\rangle \approx c_t n_t \delta_t (C_{t,n} - C_{t,s})(K_t^2/2)[1 + (K_t^2/2)]^{-1/2} \quad (26)$$

$$\langle L\rangle \approx n_t \delta_t [C_{t,s} + C_{t,n}(K_t^2/2)][1 + (K_t^2/2)]^{-1/2} \quad (27)$$

RESULTS

As a result implicit in the use of resistive force theory, both Ω_h and U depend linearly on the frequency f_t of rotation of the flagellum about the x-axis. This is also shown by the fact that the parameter c_t is present only in the right side of Eq. 15, and $f_t = c_t k_t/2\pi$. Given that $f_t = \Omega_t/2\pi$, also the "apparent" angular velocity Ω of rotation of the tail, $\Omega = \Omega_t - \Omega_h = 2\pi f_t - 2\pi f_h$, depends linearly on f_t. The ratios Ω/Ω_h, Ω/Ω_t, Ω/U and Ω_t/U, instead, are independent from f_t.

In Fig. 2 (solid line, left axis) is plotted the value of $f/f_h = \Omega/\Omega_h$ versus different values of the flagellar length l_t, when the flagellar beating is as depicted in Fig. 1, i.e., shaped in the form of a circular helix reversed with respect to that represented by the helical head. The values of the other geometrical parameters, corresponding to the flagellar tail and head of *Xenopus* spermatozoon, are given in Table 1. Coefficients 8 and 9 from Gray and Hancock (1955) have been used. We see that at the experimental measured value of the flagellum, ~40 μm (Table 1), the "apparent" angular velocity of the tail is ~20% of Ω_h. From measures based on photographs taken from video recordings of *Xenopus* spermatozoa, the two velocities showed, on the contrary, similar values (Table 1). According to Fig. 2, this result may be obtained with a reduced tail length of about 28 μm (* in Fig. 2, solid line). A possible reason for the discrepancy between the observed and calculated tail length will be discussed further on. Observe that at the reduced tail length the radial amplitude of a helical wave calculated according to the formula given in Table 1, still maintaining the same value of δ_t and n_t, is reduced from more than 4 μm to ~2 μm (dashed line, right axis).

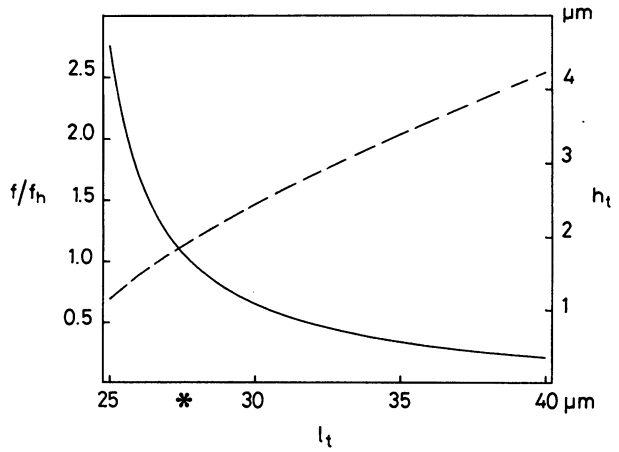

FIGURE 2 f/f_h versus l_t plots (solid line, left ordinate axis) and h_t versus l_t plot (dashed line, right ordinate axis). The * indicates the flagellar length giving the same value of f/f_h found experimentally (see Table 1). Helical flagellar pattern as in Fig. 1, Gray and Hancock (1955) force coefficients. See text for further explanations.

Fig. 2 also allows us to determine $\Omega_t/\Omega_h = \Omega/\Omega_h + 1$, or Ω_t/Ω; in this way the frequency f_t of rotation of the flagellum around its x-axis, a quantity indirectly observable, may at least in principle be estimated (see Discussion section).

In Fig. 3, A and B is plotted the ratio f_h/U versus different values of l_t, in the case of a helical (A) and a planar (B) flagellar wave. The values of the other geometrical parameters are those of Table 1. Curves (GH) are calculated using Gray and Hancock (1955) coefficients 8 and 9. The other curves are calculated according to different force coefficients. In curves L1 and L2 the coefficients $C_{t,n}$ and $C_{t,s}$ have been determined according to Lighthill's (1975) equations (Eqs. 8′, 9′), which give a ratio $C_{t,s}/C_{t,n} = 0.66$. However, both Gray and Hancock's (1955) and Lighthill's (1975) formulae hold only when $k_i h_i \ll 1$. This may be true for the flagellar tail, not for the helical head with the parameter values given in Table 1. For arbitrary values of $k_h h_h$, $C_{h,s}/C_{h,n}$ may have a value somewhat higher than 0.5 (Brokaw, 1970). For this reason we have used values that are both larger than 0.66, i.e., $C_{h,s}/C_{h,n} = 0.7$ (L1) and $C_{h,s}/C_{h,n} = 0.8$ (L2). These values, even if arbitrary, may give an idea of the effect of increasing the ratio of the force coefficients. For the GH curve of Fig. 3 A, we see that for the measured tail length of 40 μ the value of f_h/U is about 0.4 μm^{-1}, against the value of 0.21 μm^{-1} observed experimentally. However, for the abovementioned value of $l_t = 28$ μm (*) the theoretical value decreases to 0.267 μm/s, not too far from the experimental data. In the case of curves L1 and L2 of Fig. 3 A, the fit to the experimental values is still worse.

In Fig. 4 is a plot of f_h/U versus l_t when the direction of rotation of the flagellum around the x-axis is inverted with respect to the situation illustrated in Fig. 1, i.e., when the flagellum has the same sense of rotation of the head. Observe the great increase of the ratio f_h/U with respect to the previous case represented in Fig. 3 A (curve GH).

In Fig. 5 different linear plots of f_h versus U are shown, corresponding to a tail length of 40 μm, calculated in the case of helical (hw, hw′) and planar (pw) flagellar waves, compared with the curve fitted to the experimental data taken from Fig. 6 of Bernardini et al. (1988). The ratio of the force coefficients has been determined according to the Gray and Hancock (1955) theory for hw and pw, and with an increased

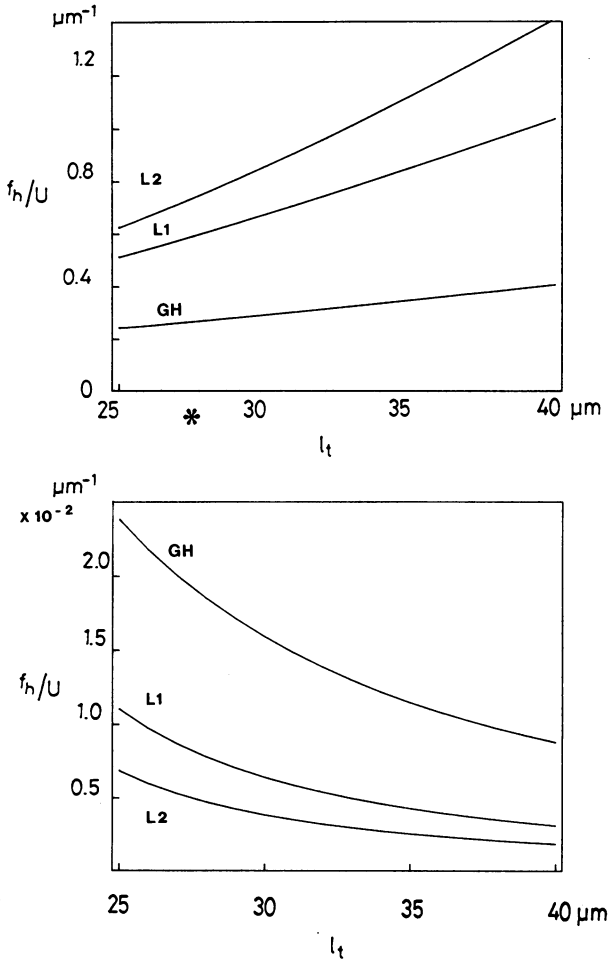

FIGURE 3 f_h/U versus l_t plots for spermatozoa with helical head and helical flagellar wave (A) and planar flagellar wave (B). GH, Gray and Hancock (1955) force coefficients; *, flagellar length giving a f_h/U value close to that found experimentally. Lighthill (1975) force coefficients for the flagellar tail (L1, L2): $C_{h,s}/C_{h,n} = 0.7$ (L1), $C_{h,s}/C_{h,n} = 0.8$ (L2). Helical pattern of flagellar beating in (A) as in Fig. 1. Other explanations in the text.

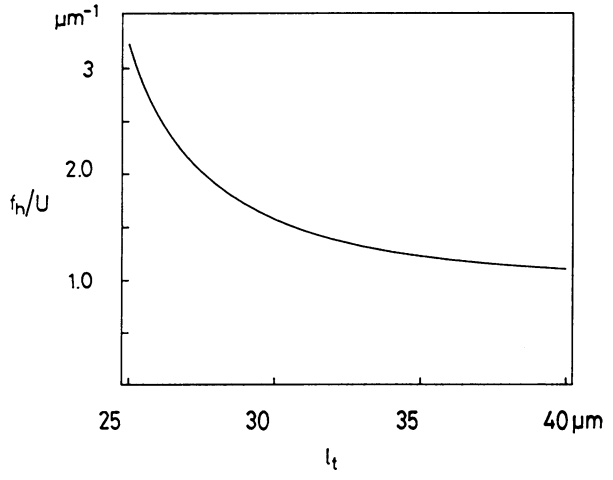

FIGURE 4 f_h/U versus l_t plot for spermatozoa with an inverted helical pattern of the flagellar beating. Gray and Hancock (1955) force coefficients. Geometrical parameter values as in Fig. 2.

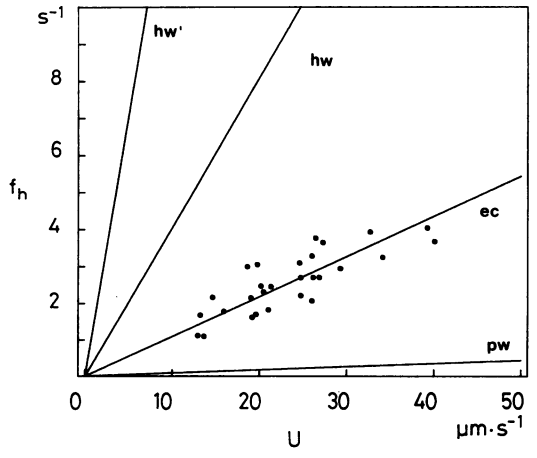

FIGURE 5 f_h versus U plots for spermatozoa with $l_t = 40$ μm: hw, hw', helical flagellar wave; pw, planar flagellar wave; ec, curve fitted to experimental data (●). The force coefficients are calculated according to Gray and Hancock (1955) for hw, pw; as in L2 of Fig. 3 for hw'. The values of the geometrical parameters of the flagellar tail and head are those of Table 1.

value of the force coefficient ratios, as in L2 of Fig. 3, for hw'. This same increased ratio for the case of a planar flagellar wave gives rise to a curve below pw, not represented in the figure.

In Fig. 6 different plots of f_t/U versus l_t are shown. A first one (hh), corresponding to a sperm with a helical flagellar beating and a helical head, is calculated according to Eq. 15. Observe that the curve reaches a minimum at about 33 μm. If we assume that the value of f_t is proportional to the energy required to move the flagellum, this flagellar length should be that which requires a minimum power for propelling the spermatozoon. A second plot (hs), for the case of a spermatozoon with a spherical head with the same volume of the helical one, is calculated according to Eq. 35 of Chwang and Wu (1971).

The reason for the increase in the propulsion efficiency of spermatozoa with helical heads, with respect to those provided with spherical ones, should be related to the fact that the first kind of heads not only exert a resistive effect against the fluid but also a propulsive one, owing to the rotation induced by the helical movement of the flagellum, caused by the head spinning in the fluid. In fact the experimental curve (ec) of Fig. 5 matches very closely that of an "ideal" screw, with the same pitch of the spermatozoon head, advancing in the medium without slipping. In fact, this coincidence is only casual, and the experimental curve should be the result of a compromise between the situation of a spermatozoon with helical flagellar waves (hw in Fig. 5), which spins much more rapidly than the ideal screw, and that of a spermatozoon with a planar flagellar wave (pw in Fig. 5), which spins much more slowly.

In Fig. 6 are also shown f_t/U versus l_t plots in the case of planar waves. One of them corresponds to a spermatozoon with a helical head (ph), and is calculated according to Eqs.

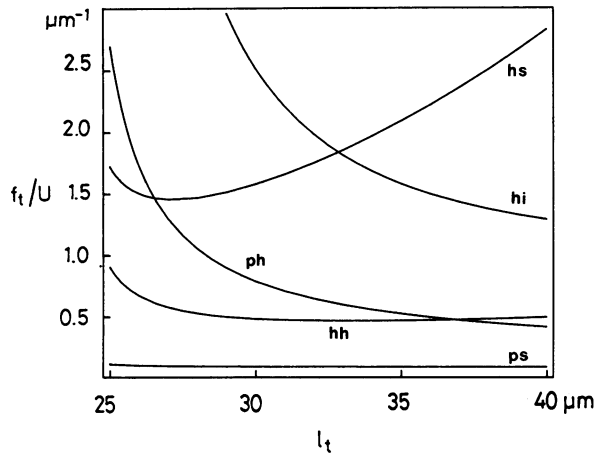

FIGURE 6 f_t/U versus l_t plots for spermatozoa with: helical flagellar wave and helical head (hh, hi), helical flagellar wave and spherical head (hs), planar flagellar wave and helical head (ph), and planar flagellar wave and spherical head (ps). Helical pattern of the flagellar beating: hh, hs, ph, ps, as in Fig. 1; hi, reversed. Gray and Hancock (1955) force coefficients. The values of the geometrical parameters of the flagellar tail and head are those of Table 1.

21 and 25, making allowance for Eqs. 26 and 27. A second plot (ps), concerning a spermatozoon with a spherical head with the same volume of the helical one, has been calculated according to approximate formulas given previously by Gray and Hancock (1955). For planar waves the propulsion efficiency of the tail does not reach any maximum in the range of flagellar length considered, because it increases monotonically with l_t. Contrary to what has been observed in the case of helical flagellar waves, in the case of planar waves the spermatozoa with helical heads are shown to be far less efficient than those provided with spherical ones. This is because, in such a situation, owing to the low speed of rotation, the contribution of a helical head shape to the advancing of the organism is very low and it is not able to counterbalance its increased resistance to the propulsive force.

A last plot of Fig. 6 (hi) represents the case when the direction of rotation of the flagellar beating is reversed as in Fig. 4.

DISCUSSION

A rigorous analysis of the kinematics of *Xenopus* sperms' motion should probably reveal that they move following a helical path, like many other similar organisms. Their trajectory should be characterized by their own pitch, radius, and angular frequency and analyzed according to these parameters (see, e.g., Crenshaw (1989)). In fact, in a first approximation the trajectories followed by *Xenopus* sperms appear to be quite straight, and the present analysis will account only for the two more important parameters that characterize the sperms' movement, i.e., their translational and rotational velocities (U and Ω_h, respectively).

By inspection of photographs taken from video recordings of *Xenopus* spermatozoa we have observed that the amplitude of the flagellum lateral displacement seems to decrease or to increase slightly during rotation. This is not what we would expect for a planar sinusoidal or circular helical flagellar beating. However, it could be consistent with a flattened helical pattern with an elliptical or oval y-z projection. Observe that to have a circular helix with a reduced value of h_t, by still maintaining the same value of δ_t and n_t, we have to reduce the value of l_t as is shown in Fig. 2 (dashed line, right axis). On the other hand, video recording or direct observation may not discriminate unequivocally between a planar or a three-dimensional flagellar beating. In fact, because of the rotation of the whole sperm induced by the head, even a planar wave should "look" three-dimensionally shaped. An indirect evidence of an effective three-dimensional flagellar beating (Bernardini et al., 1988) should be confirmed on the basis of the present theoretical analysis.

In general the rapid sperm motion prevents accurate and quick measurements of (apparent) flagellar beat frequency f. However, when a lower mobility in a high-osmolarity medium is induced (Bernardini et al., 1988), more reliable measurements may be performed. From a series of video recordings in such a situation we have observed that the spermatozoon head shows a yawing motion. A similar oscillation has been observed in other cases in flagellate organisms (Holwill, 1965), and it could originate from a transversal component because of asymmetries arising in the course of the flagellar beating. We have already said that such a yawing should be expected for a planar flagellar beating. In the three-dimensional case, the transversal component should be less relevant, at least in the case of a circular helical pattern of flagellar beating. It could be quite relevant, instead, for a flattened or elliptical helix. In our case of induced slow mobility, pitches showed a frequency of about 1 Hz, correlated to a value of both f and f_h of about 0.5 Hz. In this condition the theory predicts $f_t = f + f_h = 1$ Hz. This fact seems to indicate what we would expect, i.e., that the head pitching is correlated to the frequency of rotation of the flagellum around the x-axis. Because the evaluation of the yawing frequency is much easier to perform than the direct measure of the flagellar beating frequency, it may give a more reliable method to determine f_t.

Microphotographs seem to show a direction of rotation of the flagellum contrary to that observed in the head. This is also what we would expect on a theoretical ground, to increase the efficiency of the propulsion (Fig. 6, compare curves hi and hh) and by comparing Figs. 3 *A*, and 4 and the experimental curve (ec) of Fig. 5.

Experimental measured values of f_h versus U are fitted by a linear plot that is intermediate to those relative to helical and planar flagellar waves (Fig. 5), but nowhere close to either of them. The difference between theoretical and experimental curves may not be attributed to the use of nonsuitable force coefficients, because according to other coefficient ratios the f_h/U slope is still higher in case of helical flagellar beating (compare GH, L1, and L2 of Fig. 3 *A*, and hw and hw′ of Fig. 5) and still smaller for planar flagellar beating (compare GH, L1, and L2 of Fig. 3 *B*). The result of

the present analysis is consistent with the fact that the flagellar beating of *Xenopus* spermatozoa is effectively three-dimensional and nonplanar. However, it is not consistent with the assumption of a circular helical wave. Given that this difference should not depend on the use of nonsuitable force coefficient ratios, it could be attributed to a different geometry of the (three-dimensional) flagellar shape. We suggest here, as a possibility that we hope to explore in a future work, a shape conforming to a flattened helix, with an elliptical y-z projection.

A last point to stress is that, in the case of a (circular) helical flagellar beating, the helical shape of the head seems to increase considerably the velocity of propulsion of the spermatozoon, with respect to the energy expenditure, compared with the more common spherical shape, as we see in Fig. 6 (curves hs and hh). On the contrary, in the case of planar flagellar waves, a helical head decreases, instead of increases, movement efficiency (Fig. 6, curves ps and ph). Regarding helical and planar flagellar waves, the first ones seem to be far less efficient than the second ones, in the case of spherical heads (Fig. 6, curves hs and ps). This result is the opposite of that shown by Chwang and Wu (1971) in their Fig. 10. However, the conditions are not comparable, because the parameter values of Table 1 are very different from those giving optimal results for helical waves. Instead, in the case of helical heads, there is no definite advantage, in terms of efficiency, in having planar or helical flagellar waves (Fig. 6, curves hh and ph); for higher values of tail length there is a greater efficiency with a planar wave, for smaller values, on the contrary, with a helical one. This result does not change, at least qualitatively, when using different force coefficients (plots not presented here).

REFERENCES

Bernardini, G., F. Andrietti, M. Camatini, and M. P. Cosson. 1988. *Xenopus* spermatozoon: correlation between shape and motility. *Gamete Res.*. 20: 165–175.

Brokaw, C. J. 1970. Bending moments in free-swimming flagella. *J. Exp. Biol.* 53:445.

Brown, H. P. 1945. On the structure and mechanics of the protozoan flagellum. *Ohio J. Sci.* 45:247–301.

Chwang, A. T., and T. Y. Wu. 1971. A note on the helical movement of microorganisms. *Proc. R. Soc. Lond. B. Biol. Sci.* 178:327–346.

Chwang, A. T., T. Y. Wu, and H. Winet. 1972. Locomotion of spirilla. *Biophys. J.* 12:1549–1561.

Crenshaw, H. C. 1989. Kinematics of helical motion of microorganisms capable of motion with four degrees of freedom. *Biophys. J.* 56: 1029–1035.

Gray, J., and Hancock, G. J. 1955. The propulsion of sea urchin spermatozoa. *J. Exp. Biol.* 32:802–814.

Higdon, J. J. L. 1979. A hydrodynamic analysis of flagellar propulsion. *J. Fluid Mech.* 90:685–711.

Holwill, M. E. J. 1965. The motion of *Strigomonas oncopelti*. *J. Exp. Biol.* 42:125–137.

Holwill, M. E. J. 1966. The motion of *Euglena viridis*: the role of flagella. *J. Exp. Biol.* 44:579–588.

Lamb, H. 1932. Hydrodynamics. Cambridge University Press, Cambridge, U. K.

Lowndes, A. J. 1943. The swimming of unicellular flagellate organisms. *Proc. Zool. Soc. Lond.* 113:99–107.

Lighthill, J. L. 1975. Mathematical Biofluid Dynamics. SIAM, Philadelphia. 281 pp.

Mysercough, M. R., and M. A. Swan. 1989. A model for swimming unipolar spirilla. *J. Theor. Biol.* 139:201–218.